The Emerald Research Register for this journal is available at
www.emeraldinsight.com/researchregister

The current issue and full text archive of this journal is available at
www.emeraldinsight.com/0961-5539.htm

Received July 2003
Revised April 2004
Accepted June 2004

Conjugate turbulent forced convection in a channel with an array of ribs

K.J. Hsieh and F.S. Lien
Department of Mechanical Engineering, University of Waterloo, Waterloo, Ontario, Canada

Abstract

Purpose – Performance of various k-ε models on turbulent forced convection in a channel with periodic ribs is assessed.

Design/methodology/approach – The influence of the Yap correction and the non-linear stress-strain relation on the predictions of mean-flow, turbulence quantities and local heat transfer rate is examined. The effect of thermal boundary conditions on the heat transfer predictions is investigated by employing both the prescribed heat flux approach and the conjugate heat transfer approach.

Findings – It was found that the inclusion of the Yap correction in the ε-equation significantly improves the predictions of mean velocity and wall heat transfer for both high-Reynolds number and low-Reynolds number k-ε models in the present ribbed channel flow with massive flow separation. The employment of the non-linear stress-strain relation only marginally improves the predictions of turbulence quantities: the turbulence anisotropy is reproduced although the level of turbulence intensity is still too low. In general, the conjugate heat transfer approach predicts better average Nusselt number than the prescribed heat flux approach. However, both approaches under-predict the experimental value by about 28-33 percent when the low-Reynolds number k-ε model of with the Yap term is adopted.

Originality/value – Thorough numerical treatments of the thermal boundary conditions at the solid-liquid interface, and detailed periodic condition in the periodic regime, were given in the paper to benefit researchers interested in solving similar problems.

Keywords Convection, Heat transfer, Channel flow

Paper type Research paper

Nomenclature

C_1, C_2, C_3 = coefficients of the non-linear stress-strain relation
$C_{\varepsilon 1}, C_{\varepsilon 2}$ = coefficients in the ε-equation
C_μ = coefficient in the eddy viscosity formula
C_p = specific heat
D = channel height
D_h = hydraulic diameter
f_1, f_2 = coefficients in the ε-equation for low-Reynolds number (LRN) models
f_μ = damping function in the eddy viscosity formula for LRN models
H = rib height
k = turbulent kinetic energy
$\dot{m}$ = mass flux
n = surface normal
$\underline{\mathrm{Nu}}$ = local Nusselt number
$\overline{\mathrm{Nu}}$ = average Nusselt number
P = pressure
$\tilde{P}$ = periodic part of pressure
Pi = rib pitch

The authors gratefully acknowledge the financial support from Material and Manufacturing Ontario through MMO Project #DE708.

International Journal of Numerical Methods for Heat and Fluid Flow
Vol. 15 No. 5, 2005
pp. 462-482
© Emerald Group Publishing Limited
0961-5539
DOI 10.1108/09615530510593648

P_k = turbulence production term in the k-equation
P'_k = modification of P_k
Pr = Prandtl number
$\mathrm{Pr_t}$ = turbulent Prandtl number
q_w = wall heat flux
Re = Reynolds number
$\mathrm{Re_t}$ = turbulent Reynolds number
S = strain-rate invariant
S_{ij} = strain-rate tensor
T = temperature
$\tilde{T}$ = periodic part of temperature
T_b = bulk temperature
u_j = velocity components in the x_j direction
u_{rms} = turbulence intensity in the x direction ($u_{rms}{}' = \sqrt{\overline{u'u'}}$)
u_τ = friction velocity
$\overline{u_i'u_j'}$ = Reynolds stress
$\overline{u_j'T'}$ = turbulent heat flux
U_b = bulk velocity
x_j = Cartesian coordinates
y^+ = $y^+ = yu_\tau/\nu$
y^* = $y^* = y\sqrt{k}/\nu$

Greek symbols
α = thermal diffusivity
β = pressure gradient
δ_{ij} = Kronecker's delta
ε = dissipation rate of k
γ = temperature gradient
κ = von Karman constant
λ = thermal conductivity
λ' = thermal conductivity ratio of solid to fluid
ν = kinematic viscosity
ν_t = eddy viscosity
Ω = vorticity invariant
Ω_{ij} = vorticity tensor
ϕ = variable
ρ = density
σ_ε = model constant for the ε-equation
σ_k = model constant for the k-equation
τ_w = wall shear stress
ψ = variable representing P or T in Section 3.2

1. Introduction

Forced convection in a channel with rib-roughened walls is seen in a variety of applications, including cooling of electronics, turbine blades and heat exchangers. Ribs are used to enhance heat transfer by increasing the heat transfer surface area and by interrupting the wall boundary layer to promote mixing and turbulence (Young and Vafai, 1999; Wang and Vafai, 1999). Fully developed channel flows have been extensively studied, and the experiments of Drain and Martin (1985); and Liou *et al.* (1993) have been frequently used for turbulence model validation. Drain and Martin performed laser-Doppler velocimetry measurements of the velocity field of water flow in a channel with one wall roughened by periodic ribs. Liou *et al.* conducted the corresponding heat transfer measurements for the same geometry in an airflow using the holographic interferometry technique. The most recent numerical studies on these two cases include Bredberg and Davidson (1999), Manceau *et al.* (2000) and Tsai *et al.* (2000).

Various thermal boundary conditions have been adopted to investigate the heat transfer along the ribbed wall in order to compare with Liou *et al.*'s measurements, in which the wall was constructed of aluminum and heated by a thermal film attached to its underside. Bredberg and Davidson and Manceau *et al.* imposed one-third of the heat flux on each of the rib faces to avoid solving the conjugate conduction-convection problem. In essence, they assumed that the heat flux entering the rib base from the channel wall was equally distributed through the rest of the rib faces. In addition to the above prescribed heat flux approach, Manceau *et al.* also adopted the conjugate heat transfer approach to solve conduction and convection equations simultaneously. However, no details were given about how the conjugate problem was solved.

The near-wall treatments of turbulence models are key factors to yield accurate wall heat transfer predictions. In the high-Reynolds number (HRN) k-ε models, wall functions are commonly employed to bridge the turbulent and near-wall viscous regions. However, for non-equilibrium separated flows, the validity of the wall-function approach, particularly when heat transfer prediction is the primary interest, is questionable. In the low-Reynolds number (LRN) k-ε models, damping functions are used to mimic the physical damping on turbulence by walls. One well-known problem of most LRN models is that they tend to predict excessive near-wall turbulence length scale, and Yap (1987) proposed a correction to this problem by introducing an extra source term into the ε-equation to drive near-wall length scale towards its local equilibrium value.

In the conventional eddy-viscosity turbulence models, the linear stress-strain relation based on the Boussinesq approximation is commonly used, which can result in isotropic Reynolds normal stresses even in simple shear flows. To overcome this deficiency, each Reynolds normal stress can be solved from its own transport equation containing convection, diffusion, production, dissipation and pressure-strain processes, the last being responsible for the redistribution of turbulence energy among its three normal stress components. Unfortunately, this modeling approach, referred to as second-moment closure model, suffers from poor numerical stability and high computational cost. A potential alternative to second-moment closure, while retaining the advantageous elements of the linear eddy-viscosity framework, is to express the Reynolds stresses in terms of a non-linear expansion in powers of strain-rate and vorticity tensors explicitly (Pope, 1975) – hence the term "non-linear eddy-viscosity model". Examples include the model of Shih *et al.* (1993) and Speziale (1987).

In the present study, the standard HRN k-ε model with wall functions and the LRN k-ε model of Lien and Leschziner (1999), both combined with the Yap correction term, are validated against the measurements of Drain and Martin (1985) and Liou *et al.* (1993). The effect of thermal boundary conditions on the heat transfer predictions is investigated by employing both the prescribed heat flux approach and the conjugate heat transfer approach. In the latter, the influence of the thermal conductivity ratio of solid to fluid is also considered. To examine the effect of turbulence anisotropy on the mean-flow and heat transfer predictions, the "realizable" non-linear k-ε model of Shih *et al.* (1993) is adopted.

2. Mathematical formulation

2.1 Governing equations

The Reynolds (time-averaged) continuity, momentum, and energy equations for steady incompressible flows can be written, in Cartesian tensor notation, as

$$\frac{\partial}{\partial x_j}(u_j) = 0 \tag{1}$$

$$\frac{\partial}{\partial x_j}(u_j u_i) = -\frac{1}{\rho}\frac{\partial P}{\partial x_i} + \frac{\partial}{\partial x_j}\left[\nu\left(\frac{\partial u_i}{\partial x_j} + \frac{\partial u_j}{\partial x_i}\right) - \overline{u_i' u_j'}\right] \tag{2}$$

$$\frac{\partial}{\partial x_j}(u_j T) = \frac{\partial}{\partial x_j}\left(\alpha\frac{\partial T}{\partial x_j} - \overline{u_j' T'}\right) \tag{3}$$

where u_j is the time-averaged velocity in the x_j-direction, with $j = 1$ or 2 representing the streamwise x or vertical y direction; viz. $(x_1, x_2) \equiv (x, y)$ and $(u_1, u_2) \equiv (u, v)$.

2.2 Turbulence models

In the two-equation k-ε models, the Reynolds stresses ($\overline{u_i' u_j'}$) and turbulent heat fluxes ($\overline{u_j' T'}$) are modeled in terms of the eddy viscosity (ν_t), turbulent kinetic energy (k) and its dissipation rate (ε). Based on series-expansion arguments by Pope (1975), the stress-strain relationship can be written as

$$\frac{\overline{u_i' u_j'}}{k} = \frac{2}{3}\delta_{ij} - \underbrace{\frac{\nu_t}{k} S_{ij}}_{\text{linear term}} + \underbrace{C_1 \frac{\nu_t}{\varepsilon}\left(S_{ik}S_{kj} - \frac{1}{3}\delta_{ij}S_{kl}S_{kl}\right) + C_2 \frac{\nu_t}{\varepsilon}(\Omega_{ik}S_{kj} + \Omega_{jk}S_{ki}) + C_3 \frac{\nu_t}{\varepsilon}\left(\Omega_{ik}\Omega_{jk} - \frac{1}{3}\delta_{ij}\Omega_{kl}\Omega_{kl}\right)}_{\text{quadratic term}} + \text{HOT} \tag{4}$$

where HOT denotes higher order terms,

$$\nu_t = \begin{cases} C_\mu \frac{k^2}{\varepsilon} & \text{for HRN } k\text{-}\varepsilon \text{ models} \\ C_\mu f_\mu \frac{k^2}{\varepsilon} & \text{for LRN } k\text{-}\varepsilon \text{ models} \end{cases} \tag{5}$$

and

$$S_{ij} = \frac{\partial u_i}{\partial x_j} + \frac{\partial u_j}{\partial x_i}, \quad \Omega_{ij} = \frac{\partial u_i}{\partial x_j} - \frac{\partial u_j}{\partial x_i} \tag{6}$$

In the conventional linear formulation of the eddy viscosity models, $C_\mu = 0.09$ and the coefficients C_1 to C_3 are all zero. The non-linear strain-stress relation (NLSS) was proposed by including the products of the strain-rate and vorticity tensors up to the quadratic term or higher into the Reynolds stresses. Many forms of the quadratic term have been proposed, and the C_μ, C_1 to C_3 terms proposed by Shih *et al.* (1993) are given as

$$C_\mu = \frac{0.667}{1.25 + S + 0.9\Omega} \tag{7}$$

$$C_1 = \frac{3/4}{(1000 + S^3)C_\mu}, \quad C_2 = \frac{15/4}{(1000 + S^3)C_\mu}, \quad C_3 = \frac{19/4}{(1000 + S^3)C_\mu} \tag{8}$$

where

$$S = \frac{k}{\varepsilon}\sqrt{\frac{1}{2}S_{ij}S_{ij}}, \quad \Omega = \frac{k}{\varepsilon}\sqrt{\frac{1}{2}\Omega_{ij}\Omega_{ij}} \tag{9}$$

The damping function (f_μ) in equation (5) will be defined in Section 2.2.2. The turbulent heat fluxes are modeled using the Boussinesq approximation as

$$\overline{u_j' T'} = -\frac{\nu_t}{\mathrm{Pr_t}} \frac{\partial T}{\partial x_j} \tag{10}$$

where $\mathrm{Pr_t} = 0.9$ is the turbulent Prandtl number used in wall-bounded flows.

2.2.1 High-Reynolds number k-ε model with wall functions. The governing equations for the HRN k-ε model are written as

$$\frac{\partial}{\partial x_j}(u_j k) = \frac{\partial}{\partial x_j}\left(\frac{\nu_t}{\sigma_k}\frac{\partial k}{\partial x_j}\right) + P_k - \varepsilon \tag{11}$$

$$\frac{\partial}{\partial x_j}(u_j \varepsilon) = \frac{\partial}{\partial x_j}\left(\frac{\nu_t}{\sigma_\varepsilon}\frac{\partial \varepsilon}{\partial x_j}\right) + \frac{\varepsilon}{k}(C_{\varepsilon 1} P_k - C_{\varepsilon 2}\varepsilon) \tag{12}$$

where $\sigma_k = 1.0$, $\sigma_\varepsilon = 1.3$, $C_{\varepsilon 1} = 1.44$ and $C_{\varepsilon 2} = 1.92$ are model constants recommended by Launder and Spalding (1974). The turbulence production term (P_k) in the k-equation is defined as

$$P_k = -\overline{u_i' u_j'}\frac{\partial u_i}{\partial x_j} \tag{13}$$

Wall functions, which are based on the logarithmic law of the wall, assume that the near-wall region consists of two layers: the inner layer which extends from the wall up to $y^+ = 11.63$, and the outer layer where $y^+ > 11.63$. The dimensionless wall-normal distance is given by $y^+ = y u_\tau / \nu$ where $u_\tau = \sqrt{\tau_\mathrm{w}/\rho}$ is the friction velocity and τ_w is the wall shear stress. In the outer layer, the velocity and temperature profiles are given by

$$u^+ = \frac{\ln(E y^+)}{\kappa}, \quad T^+ = \mathrm{Pr_t}(u^+ + \mathrm{Pee}) \tag{14}$$

where $\kappa = 0.42$ is the von Karman constant and $E = 9.8$ is an integration constant for smooth walls. The Pee term is a function that depends on the ratio of laminar to turbulent Prandtl number. Jayatilleke (1969) proposed

$$\mathrm{Pee} = 9.24\left[\left(\frac{\mathrm{Pr}}{\mathrm{Pr_t}}\right)^{0.75} - 1\right] \times \left[1 + 0.29\ \exp\left(-0.007\frac{\mathrm{Pr}}{\mathrm{Pr_t}}\right)\right] \tag{15}$$

where $\mathrm{Pr} = 0.71$ is the Prandtl number for air.

2.2.2 Low-Reynolds number k-ε model. Jones and Launder (1972) first proposed a LRN k-ε model by introducing damping functions based on the local turbulent Reynolds number ($\mathrm{Re_t} = k^2/\nu\varepsilon$). Many researchers have proposed numerous variants of the LRN model, and the differences between various models are the values of model constants and the formulae of damping functions. In the version of Lien and Leschziner (1999), denoted by Model LL hereafter, the turbulence equations are written as

$$\frac{\partial}{\partial x_j}(u_j k) = \frac{\partial}{\partial x_j}\left[\left(\nu + \frac{\nu_t}{\sigma_k}\right)\frac{\partial k}{\partial x_j}\right] + P_k - \varepsilon \tag{16}$$

$$\frac{\partial}{\partial x_j}(u_j \varepsilon) = \frac{\partial}{\partial x_j}\left[\left(\nu + \frac{\nu_t}{\sigma_\varepsilon}\right)\frac{\partial \varepsilon}{\partial x_j}\right] + \frac{\varepsilon}{k}[C_{\varepsilon 1} f_1 (P_k + P'_k) - C_{\varepsilon 2} f_2 \varepsilon] + \text{Yap} \tag{17}$$

where $f_1 = 1, f_2 = 1 - 0.3\exp(-\text{Re}_t^2)$ and

$$\text{Yap} = \max\left[0.83\left(\frac{k^{3/2}}{2.5\varepsilon y} - 1\right)\left(\frac{k^{3/2}}{2.5\varepsilon y}\right)^2 \frac{\varepsilon^2}{k}, 0\right] \tag{18}$$

The damping function (f_μ) in equation (5), which is a function of dimensionless wall-normal distance $y^* = y\sqrt{k}/\nu$, is used to model the damping effect associated with pressure-strain correlations in the vicinity of walls. The damping function is defined as

$$f_\mu = [1 - \exp(-0.0198 y^*)]\left(1 + \frac{5.29}{y^*}\right) \tag{19}$$

The P'_k term in the ε-equation is introduced to ensure that the correct level of near-wall turbulence energy dissipation is returned, where

$$P'_k = \frac{C_{\varepsilon 2}}{C_{\varepsilon 1}}\left(P_k + 2\nu\frac{k}{y^2}\right)\ \exp(-0.00375 y^{*2}) \tag{20}$$

3. Numerical details

3.1 Problem description

The geometry of the ribbed channel is shown in Figure 1, where the rib pitch to rib height ratio is $\text{Pi}/H = 7.2$ and the channel height-to-rib height ratio is $D/H = 5$. The measurements of Drain and Martin (1985) and Liou *et al.* (1993) were conducted at a Reynolds number based on the bulk mean velocity and hydraulic diameter (twice the channel height) of 37,200 for the flow fields and of 12,600 for the thermal field. In the experiment of Liou *et al.* the channel top wall was insulated and the bottom wall was heated by a constant heat flux (q_b).

3.2 Periodic condition

The geometry shown in Figure 1 has a repeated pattern from pitch to pitch. At a distance sufficiently downstream in the streamwise direction, the flow becomes fully developed and periodic. Under these conditions, the calculation can be performed using only one of those identical geometrical modules to save computational time. For the present study the region between two dashed lines shown in Figure 1 is chosen as the computational domain.

All solution variables in the periodic regime, except for the pressure and temperature, are identical at the inlet and outlet of the module. The periodic relationship can be written as

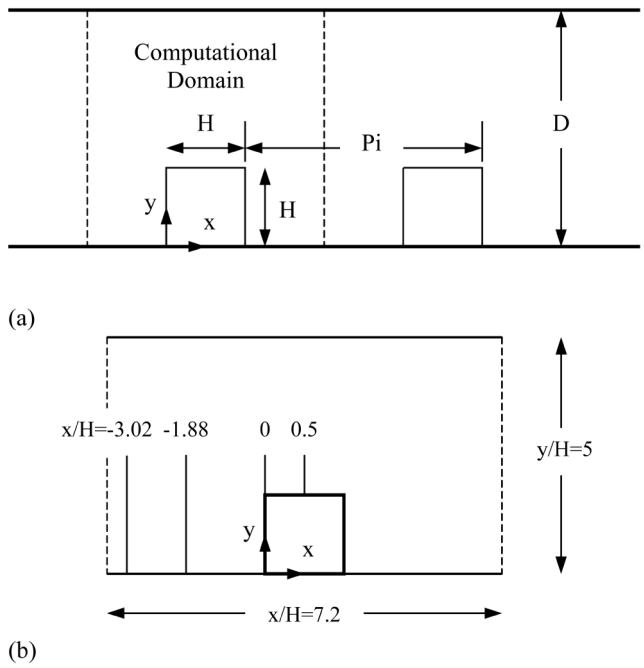

Figure 1.
Schematic of (a) the ribbed channel geometry and (b) the computational domain

$$\phi(x_{\text{inlet}}, y) = \phi(x_{\text{inlet}} + \text{Pi}, y) \tag{21}$$

where $\phi = u, v, k$ and ε.

Along the streamwise direction, the pressure drop and temperature increase across each module are constant

$$\psi(x_{\text{inlet}} + \text{Pi}, y) - \psi(x_{\text{inlet}}, y) = \text{a constant} \tag{22}$$

where $\psi = P$ or T. According to Patankar *et al.* (1977), the pressure and temperature can be decomposed into

$$P(x, y) = \tilde{P}(x, y) - \beta x \tag{23}$$

$$T(x, y) = \tilde{T}(x, y) + \gamma x \tag{24}$$

where the tilde sign represents the periodic part of the variable which satisfies equation (21), and β and γ are the pressure gradient and temperature gradient across one pitch, respectively. Substitution of equations (23) and (24) into equations (2) and (3) yields the following momentum and energy equations under the periodic condition

$$\frac{\partial}{\partial x_j}(u_j u_i) = -\frac{1}{\rho}\frac{\partial \tilde{P}}{\partial x_i} + \frac{\partial}{\partial x_j}\left[\nu\left(\frac{\partial u_i}{\partial x_j} + \frac{\partial u_j}{\partial x_i}\right) - \overline{u_i' u_j'}\right] + \beta\delta_{i1} \tag{25}$$

$$\frac{\partial}{\partial x_j}\left(u_j \tilde{T}\right) = \frac{\partial}{\partial x_j}\left[\left(\frac{\nu}{\mathrm{Pr}} + \frac{\nu_\mathrm{t}}{\mathrm{Pr_t}}\right)\frac{\partial \tilde{T}}{\partial x_j}\right] - \gamma u_i \delta_{i1} \tag{26}$$

For a given Reynolds number, there is a corresponding pressure drop. The pressure gradient β is unknown a priori and is guessed by an arbitrary constant during the first iteration. After the solution converges, the corresponding bulk mean velocity at any x location can be evaluated as

$$U_\mathrm{b} = \left.\frac{\int u(x,y)\,\mathrm{d}y}{\int \mathrm{d}y}\right|_x \tag{27}$$

Based on the U_b value, the pressure gradient β is adjusted accordingly (for example, if U_b is lower than the experimental value, then β is increased), and the overall solution procedure is repeated until the desired Reynolds number ($\mathrm{Re} = U_\mathrm{b} D_\mathrm{h}/\nu$ in the present study) is attained.

Patankar *et al.* (1977) also expressed the temperature gradient as

$$\gamma = \frac{T(x_\mathrm{inlet} + \mathrm{Pi}, y) - T(x_\mathrm{inlet}, y)}{\mathrm{Pi}} \tag{28}$$

which can be further approximated as

$$\gamma = \frac{\overline{T}(x_\mathrm{inlet} + \mathrm{Pi}) - \overline{T}(x_\mathrm{inlet})}{\mathrm{Pi}} \tag{29}$$

where

$$\overline{T}(x) = \left.\frac{\int T(x,y)u(x,y)\,\mathrm{d}y}{\int u(x,y)\,\mathrm{d}y}\right|_{x=x_\mathrm{inlet}\ \text{or}\ x_\mathrm{inlet}+\mathrm{Pi}} \tag{30}$$

For the case of a channel with an adiabatic top wall and an isoflux (q_w) bottom wall, the temperature gradient γ can be obtained by applying a global energy balance to the control volume, as shown in Figure 2. This gives rise to the following equation,

$$q_\mathrm{w}\mathrm{Pi} = \dot{m} C_\mathrm{p}\left[\overline{T}(x_\mathrm{inlet} + \mathrm{Pi}) - \overline{T}(x_\mathrm{inlet})\right] \tag{31}$$

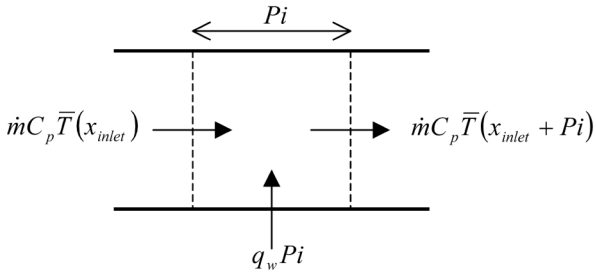

Figure 2.
Control volume for the global energy balance

Combining equations (29) and (31) results in

$$\gamma = \frac{q_w}{\dot{m} C_p} \tag{32}$$

3.3 Thermal boundary conditions

The temperature boundary condition at the heated wall can be written as

$$\left.\frac{\partial T}{\partial n}\right|_w = \left.\frac{\partial}{\partial n}\left(\tilde{T} + \gamma x\right)\right|_w = \left.\left(\frac{\partial \tilde{T}}{\partial n} + \gamma \frac{\partial x}{\partial n}\right)\right|_w = -\frac{q_w}{\lambda} \tag{33}$$

where n is the surface normal, λ is the thermal conductivity, and q_w is the heat flux at the wall.

The heat flux at the channel bottom wall is given by

$$q_w = q_b \tag{34}$$

and the mass flux is calculated as

$$\dot{m} = \rho D U_b \tag{35}$$

where $D = 5H$ and

$$U_b = \int_0^D u \, dy \Big/ \int_0^D dy$$

is the bulk mean velocity.

The temperature gradient γ is obtained by substituting equations (34) and (35) into equation (32):

$$\gamma = \frac{1}{5} \frac{q_b}{\rho C_p U_b H} \tag{36}$$

At the channel bottom wall, the boundary condition based on equations (33) and (34) is obtained as

$$\left.\frac{\partial T}{\partial n}\right|_w = \left.\frac{\partial \tilde{T}}{\partial y}\right|_w = -\frac{q_b}{\lambda} \tag{37}$$

3.3.1 Prescribed heat flux approach. Two treatments of thermal boundary conditions on a rib's surfaces are considered. The first one is to impose a constant heat flux $q_w = q_b/3$ on the rib faces. This treatment is based on the assumption that heat flux entering into the rib base from the channel wall is equally distributed to the other three faces of the rib. In this approach, the boundary conditions at the rib faces are specified as

$$\left.\frac{\partial T}{\partial n}\right|_{\mathrm{w}} = \begin{cases} \left.\frac{\partial \tilde{T}}{\partial y}\right|_{\mathrm{w}} = -\frac{1}{3}\frac{q_{\mathrm{b}}}{\lambda} & \text{at the rib top face} \\ \left.\frac{\partial \tilde{T}}{\partial x}\right|_{\mathrm{w}} + \gamma = -\frac{1}{3}\frac{q_{\mathrm{b}}}{\lambda} & \text{at the rib left and right faces} \end{cases} \tag{38}$$

3.3.2 Conjugate heat transfer approach. The second approach is to couple conduction and convection heat transfer between the rib and the fluid. This approach is computationally costly, but it ensures physical correctness. In the conjugate heat transfer problem, conduction in the solid region is coupled with convection in the adjacent fluid region. One approach to solve this problem is by solving conduction in the solid and convection in the fluid separately, followed by an iterative procedure that matches the temperature and heat flux at the solid-fluid interface.

Another way to solve this problem is to use a harmonic mean of thermal conductivity practice proposed by Patankar (1978). In this approach, the temperature equation is solved in the entire computational domain containing both the solid and fluid regions. The temperature is governed by

$$\frac{\partial}{\partial x_j}(\rho C_{\mathrm{p}} u_j T) = \frac{\partial}{\partial x_j}\left(\lambda_{\mathrm{eff}}\frac{\partial T}{\partial x_j}\right) \tag{39}$$

where λ_{eff} is the effective thermal conductivity specified as:

$$\lambda_{\mathrm{eff}} = \begin{cases} \lambda_{\mathrm{f}} - \rho C_{\mathrm{p}}\overline{u'T'} & \text{in the liquid region} \\ \lambda_{\mathrm{s}} & \text{in the solid region} \\ \lambda_{\mathrm{int}} & \text{at the solid-fluid interface} \end{cases} \tag{40}$$

and the subscripts s and f denote solid and fluid, respectively. In equation (39), only the values of fluid density and specific heat at constant pressure are employed. The values of solid density and specific heat are not used because velocities in the solid region are zero. As a result, equation (39) is solved as a pure conduction equation in the solid region.

The heat flux across the solid-fluid interface can be represented by the harmonic mean of the conductivities of the two adjacent control volumes. Consider two control volumes separated by the solid-fluid interface, shown in Figure 3, where the left control

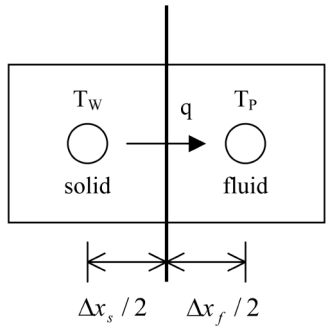

Figure 3.
Control volumes adjacent to the solid-liquid interface

volume is in the solid region and the right control volume is in the fluid region. To ensure energy conservation at the interface, the heat flux leaving the solid (denoted by q_s) must equal the heat flux entering the fluid (denoted by q_f). Based on a piecewise-linear temperature profile, the heat fluxes are defined as

$$q_s = -\lambda_s \left.\frac{\partial T}{\partial x}\right|_s = -\lambda_s \frac{T_i - T_W}{\Delta x_s/2} \tag{41}$$

$$q_f = -\lambda_f \left.\frac{\partial T}{\partial x}\right|_f = -\lambda_f \frac{T_P - T_i}{\Delta x_f/2} \tag{42}$$

The temperature at the interface is denoted by T_i, which can be evaluated by equating equations (41) and (42). This yields

$$T_i = \frac{\Delta x_s}{\Delta x_s + \lambda' \Delta x_f} T_P + \frac{\lambda' \Delta x_f}{\Delta x_s + \lambda' \Delta x_f} T_W \tag{43}$$

where $\lambda' = \lambda_s/\lambda_f$ is the thermal conductivity ratio of solid to fluid.

Substituting equation (43) into equation (42) gives an expression for the heat flux at the interface:

$$q_f = -\lambda_{int} \left.\frac{\partial T}{\partial x}\right|_{int} \tag{44}$$

where

$$\lambda_{int} = \frac{\lambda' \lambda_f (\Delta x_s + \Delta x_f)}{\Delta x_s + \lambda' \Delta x_f} \tag{45}$$

$$\left.\frac{\partial T}{\partial x}\right|_{int} = \frac{T_P - T_W}{x_P - x_W} \tag{46}$$

An expression for λ_{int} at the other rib faces can be derived in a similar manner.

At the rib base where $q_w = q_b$, the boundary condition is

$$\left.\frac{\partial T}{\partial n}\right|_w = \left.\frac{\partial \tilde{T}}{\partial y}\right|_w = -\frac{q_b}{\lambda_s} = -\frac{1}{\lambda'}\frac{q_b}{\lambda_f} \tag{47}$$

The channel bottom wall was made of aluminum in the experiment of Liou *et al.* but no information about the material of ribs was provided. Three different values of conductivity ratio, $\lambda' = 6{,}600$, 660 and 66, are considered in the present study, where $\lambda' = 6{,}600$ is the conductivity ratio of aluminum alloy 6061-T6 to air.

3.4 Numerical framework

The numerical solutions are obtained with the general non-orthogonal fully collocated finite-volume algorithm "STREAM" of Lien *et al.* (1996). It employs the SIMPLE pressure correction of Patankar and Spalding (1972) and Rhie and Chow interpolation (1983) to avoid pressure oscillations. The "QUICK" scheme of Leonard (1979) is used in

the momentum and energy equations, and the upwind difference scheme (UDS) is employed in the k- and ε-equations.

4. Results and discussion

Table I lists four different models used in the present study, where Model LL with Yap serves as the base model. Computed results of mean velocity (u) and turbulence intensity ($u'_{\mathrm{rms}} = \sqrt{\overline{u'u'}}$) at $\mathrm{Re} = 37,200$ obtained with various models are compared to the experimental data of Drain and Martin at four channel locations of $x/H = 0.1, 0.5, -3.02$ and -1.88.

For the heat transfer computations, the energy equation is solved separately from momentum equations. The flow field is calculated at $\mathrm{Re} = 12,600$ first, and then the thermal field is computed by solving the energy equation using the converged velocities. Heat transfer predictions are expressed in terms of the local Nusselt number, which is defined in Liou *et al.*'s experiment as

$$\mathrm{Nu} = \frac{q_{\mathrm{w}} D_{\mathrm{h}}}{\lambda (T_{\mathrm{w}} - T_{\mathrm{b}})} \tag{48}$$

where

$$T_{\mathrm{b}} = \int_0^{5H} T|u|y \,\mathrm{d}y \Big/ \int_0^{5H} |u|y \,\mathrm{d}y$$

is the local bulk mean temperature. Note that T_{b} used in computing the Nu along the rib left and right faces is based on the value of T_{b} at $x/H = 0$ and $x/H = 1$, respectively.

The heat transfer results are expressed in terms of the Nusselt number ratio, $\mathrm{Nu}/\mathrm{Nu}_s$, where $\mathrm{Nu}_s = 0.023\mathrm{Re}^{0.8}\mathrm{Pr}^{0.4}$ is the Nu for a turbulent flow in a smooth circular pipe from the Dittus-Boelter correlation. The abscissa in Figures 5 and 9, denoted by "s", is defined along the rib faces and channel bottom wall, where $s = 0$ corresponds to the upper-left corner of the rib. Figure 4 illustrates the s-coordinate system along the surfaces.

Models employed	Compared with the base model to investigate the effect of
Model LL + Yap (base model)	–
Model LL	Yap correction
Model LL + Yap + NLSS	Non-linear stress-strain relation
HRN k − ε model + Yap	LRN model vs 0 HRN model

Table I.
Models used in the channel flow study

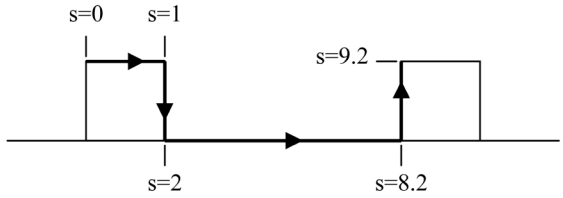

Figure 4.
Coordinate system along the solid surfaces

The average Nu (defined here as $\overline{\mathrm{Nu}} = \int_0^{9.2} \mathrm{Nu} \cdot \mathrm{ds}/9.2$) is an important parameter from engineering design point of view. $\overline{\mathrm{Nu}}/\mathrm{Nu}_s$ values from the experiment and from the various models are summarized in Table II. The $\overline{\mathrm{Nu}}$ will be discussed in Section 4.5.

4.1 Effects of grid refinement

To determine the accuracy of numerical solutions, two grids of 80×60 and 120×90 nodes are used. For LRN models, computational meshes are preferentially stretched towards the solid surfaces. For HRN models, however, only uniform grids are used. Very minor differences (less than 0.5 percent) are observed in the profiles of velocity and turbulence intensity at $\mathrm{Re} = 37,200$, and average Nusselt number at $\mathrm{Re} = 12,600$ for Model LL, and only the results obtained from the grid of 120×90 nodes are shown in the later sections unless stated otherwise. In contrast, grid refinement affects significantly the heat transfer results of the HRN k-ε model. This is because grid-spacings adjacent to walls change as the mesh is refined. Since wall functions are implemented at nodes of different heights for two different meshes and also, massive flow separation occurs in the present flow, suggesting that the y^+ values of the first nodes adjacent to walls are very low in the near-wall regions (typically less than 10 instead of in the range of 60-150 where local equilibrium condition can be assumed), it is not surprising to see that the sensitivity of numerical solutions to the change of grid density is higher than in the LRN k-ε model counterpart. In practice, grid-independent solutions for HRN models are very difficult, if not impossible, to achieve in the present case because logarithmic layer does not exist in the canyon between two consecutive ribs. Nevertheless, with the two grids examined here, the differences in terms of velocity and turbulence quantities are less than 0.5 percent, and in terms of $\overline{\mathrm{Nu}}$ is about 2.7 percent. For all results obtained with the HRN k-ε model to be shown later, the Yap term is included and calculations were performed on a mesh of 120×90 nodes.

4.2 Effects of thermal boundary conditions

The predicted Nu distributions obtained from Model LL with Yap using the prescribed heat flux approach (Section 3.3.1) and the conjugate heat transfer approach (Section 3.3.2) are shown in Figure 5. The results obtained with both approaches are almost identical along a large part of the ribbed wall (from $s = 2$ to 8.2) in the channel, with the main differences occurring at the rib faces and in the vicinity of the lower corners of the rib.

Table II.
Average Nusselt number results for the ribbed channel

	Experiment	$\overline{\mathrm{Nu}}/\mathrm{Nu}_s$
		2.04
Prescribed heat flux approach	Model LL+Yap	1.36
	Model LL	2.44
	Model LL + Yap + NLSS	1.56
	HRN k-ε model + Yap	1.89
Conjugate heat flux approach	Model LL + Yap ($\lambda' = 6{,}600$)	1.46
	Model LL + Yap ($\lambda' = 660$)	1.44
	Model LL + Yap ($\lambda' = 66$)	1.42

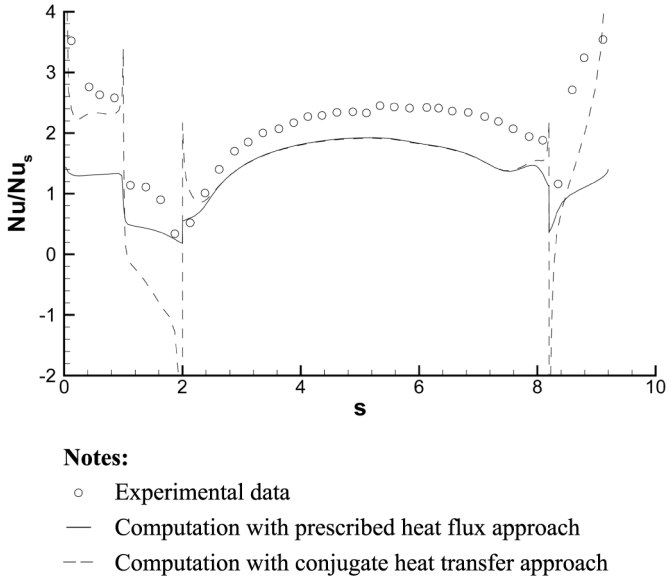

Figure 5.
Local Nusselt number distributions obtained by Model LL with Yap at Re = 12,600

It is observed that the prescribed heat flux approach predicts lower Nu than the experimental data at the rib faces. However, the results are quite satisfactory considering the simplicity of specifying $q_b/3$ at each face of the rib in contact with fluid. The results obtained with the conjugate heat transfer approach show very good agreement at the rib top face (from $s = 0$ to 1) and left face (from $s = 8.2$ to 9.2). However, negative Nu distributions are observed at the rib right face (from $s = 1$ to 2) and at the lower corner of the rib left face at around $s = 8.2$. This is because two small recirculation bubbles are observed around the lower corners of the rib shown in Figure 6, where heat is trapped in the stagnant fluid. Consequently, heat is transferred from the fluid to the rib, yielding negative Nu.

The effect of the solid-to-fluid thermal conductivity ratio on the Nu distributions for λ' being of the order of 100 or higher is negligibly small using the conjugate heat

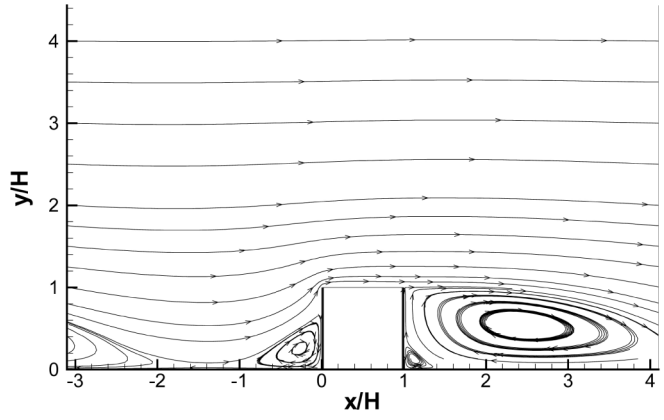

Figure 6.
Streamlines computed with Model LL + Yap at Re = 37,200

transfer approach (not shown). Young and Vafai (1998a, b) also reported that the Nu distributions become nearly identical when $\lambda' \geq 100$, which is consistent with the present observation.

In the following discussion, all the heat transfer results were obtained using the prescribed heat flux approach unless stated otherwise.

4.3 Effects of Yap correction

Two variants of Model LL, namely Model LL with and without Yap, are compared in Figure 7. It is seen from this figure that at $4 \leq y/H \leq 5$ Model LL with Yap is in good agreement with the experimental data, while Model LL without Yap slightly over-predicts the velocity profiles. At the locations of $x/H = 0.1$ and 0.5, however,

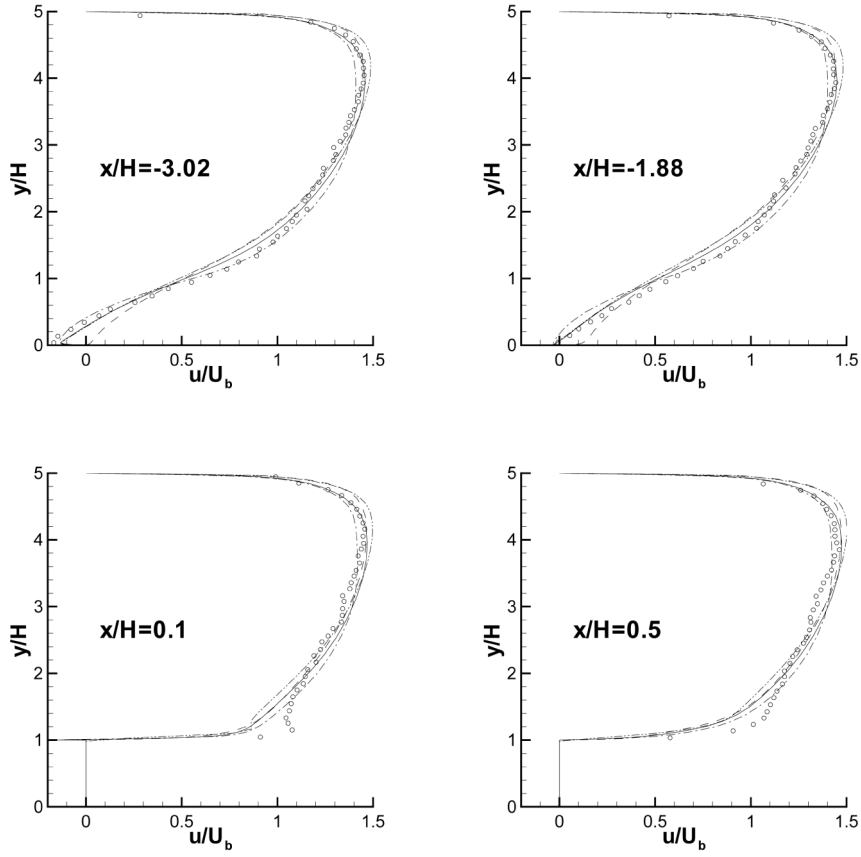

Figure 7.
Profiles of mean velocity at four channel locations at Re = 37,200

both models considerably under-predict the velocity in the region above the rib for $1 \leq y/H \leq 2$. Many researchers (e.g. Bredberg and Davidson, 1999; Manceau *et al.*, 2000; Tsai *et al.*, 2000) also found the same discrepancy, suggesting that the experiment might exhibit some three-dimensional effects.

A reversed flow is observed at the lower part of the channel at $x/H = -3.02$, and the addition of the Yap correction does improve the velocity prediction by enlarging the separation bubble there. Figure 6 shown earlier indicated that two recirculation bubbles are merged together between $x/H = -1$ and -2, and no reattachment occurs within this region. This is consistent with a very weak reversed flow observed in the velocity profile at $x/H = -1.88$ in Figure 7.

The difference between the predicted streamwise turbulence intensities from both models and the experimental data, shown in Figure 8, is large. However, this is expected from any eddy-viscosity models using the linear (Boussinesq) stress-strain relationship. The discrepancies are most significant at $x/H = -3.02$ and -1.88, and Model LL without Yap, in general, agrees slightly better with the experimental data because it tends to over-predict the turbulence energy.

Since LRN k-ε models without Yap tend to over-predict the turbulence length scale and, hence, the heat transfer rate at walls, it is seen from Figure 9 that Model LL without Yap significantly over-predicts the Nu distribution from $s = 2$ to 8.2. The inclusion of Yap in Model LL reduces the amount of turbulent energy in the near-wall region and, as a result, the heat transfer prediction is improved.

The Yap correction is originally designed as a correction term for the LRN k-ε models only. However, in the present case the y^+ values close to the bottom wall are low due to the presence of massive flow separation within the canyon of two consecutive ribs. Wall functions, described in equation (14) based on the logarithmic law of the wall, are, strictly speaking, not applicable to this region. Preliminary calculations show that the Nu returned by the standard HRN k-ε model (i.e. without including the Yap term) was too high. This deficiency was improved later when the same Yap term used in the LRN calculations was also included in the HRN model. This suggests that, if the flow is far from the local equilibrium condition (e.g. in recirculation zones), the Yap term can be introduced to LRN as well as HRN models with a drastic improvement in the heat transfer predictions. In Figures 7-10, only results obtained with the HRN k-ε model with the Yap term are shown here.

4.4 Effects of non-linear stress-strain relation

As shown in Figure 7, the base model (Model LL with Yap) with NLSS correctly predicts the velocity profile in the region $0 \leq y/H \leq 2$ at $x/H = -3.02$. However, it produces a slightly larger recirculation bubble in the wake region of the upstream rib at $x/H = -1.88$. This is because the shear-strain rate bordering the separation lines is generally large. Along these lines, the strain-rate and vorticity invariants (S and Ω) are also high, giving rise to low eddy viscosity as both S and Ω appear in the denominator of equation (7). Lower viscosity yields lower shear stress along the curved shear layer, which, in turn, reduces the amount of fluid entrained into the recirculation zone. As a result, the reversed flow is over-predicted.

In addition, the turbulence generation P_k, defined in equation (13), is also reduced because the Reynolds stresses $\overline{u_i'u_j'}$ based on Pope's constitutive equation in equation (14) are functions of eddy viscosity ν_t. This is consistent with our observations in

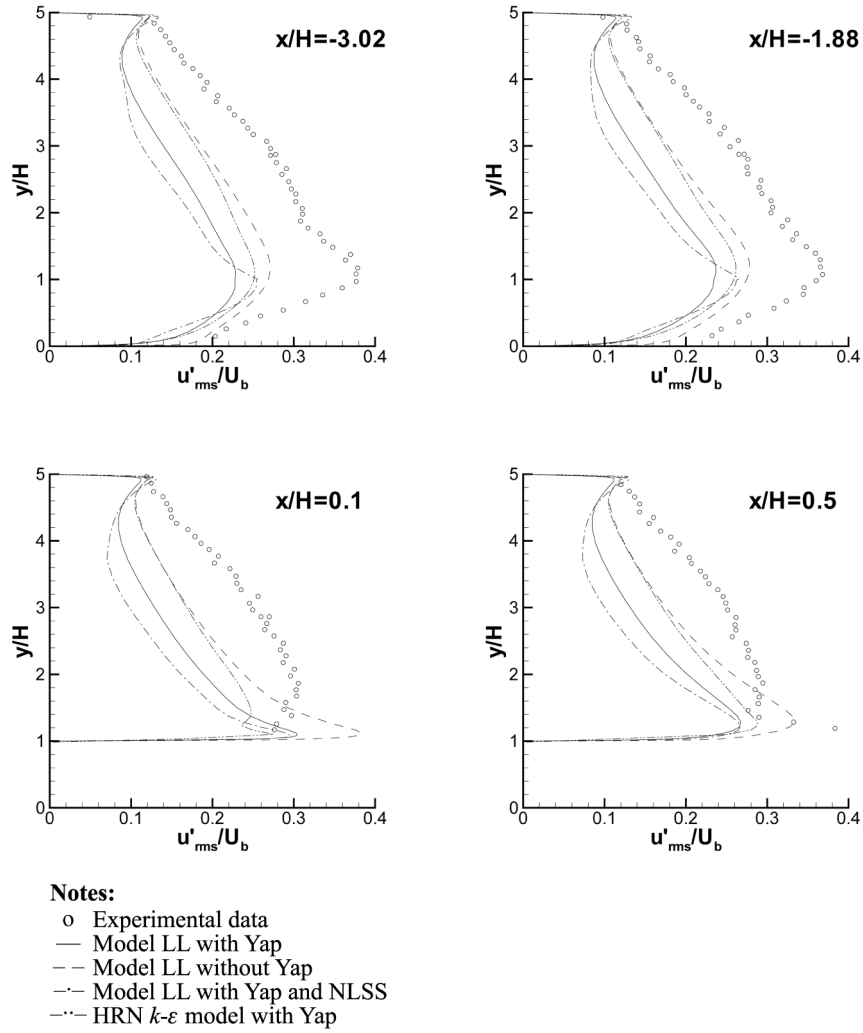

Figure 8.
Profiles of turbulence intensity at four channel locations at Re = 37,200

Figure 8 that the inclusion of the NLSS under-predicts further the turbulence intensity u'_{rms}. Even though the base model with NLSS predicts lower values of ${u_{\mathrm{rms}}}'$ at $x/H = -3.02$ and -1.88 shown in Figure 8, it presents the trend better in the region from $y/H = 0$ to 1.5. It captures the correct location of the u'_{rms} peak at $y/H \approx 1$. Model LL with NLSS also predicts better Nu distribution from $s = 4$ to 8 as seen in Figure 9.

4.5 Average Nusselt number

It is evident from Table II that, without the Yap term, the $\overline{\mathrm{Nu}}$ predicted by Model LL in conjunction with the prescribed heat flux approach, is over-predicted by about 20 percent compared to the experimental value. This is consistent with the earlier

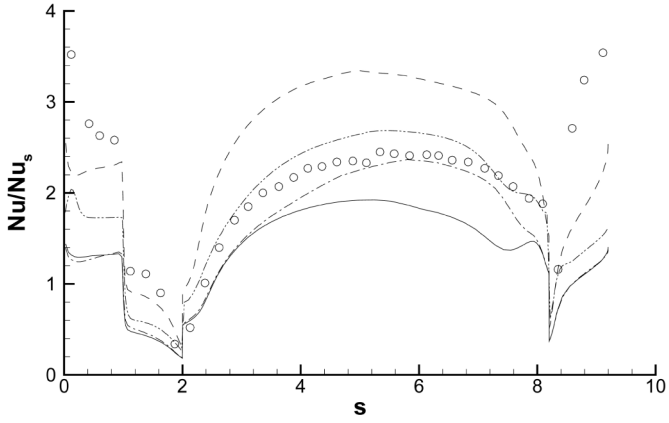

Notes:
o Experimental data
— Model LL with Yap
– – Model LL without Yap
–·– Model LL with Yap and NLSS
–··– HRN k-ε model with Yap

Figure 9.
Local Nusselt number distributions at Re = 12,600

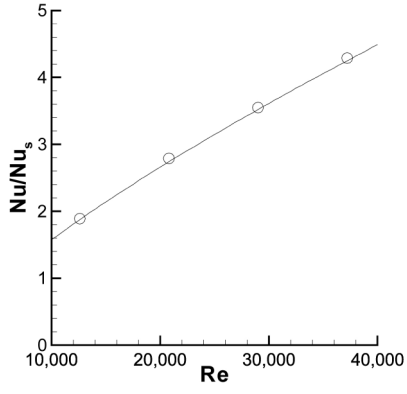

Notes:
o HRN k-ε model with Yap
— correlation of $\overline{Nu}/Nu_s = 0.0015Re^{0.7553}$

Figure 10.
Average Nusselt number at various Reynolds numbers

statement that the Yap term is designed to remedy the problem of excessive turbulent length scales near walls associated with most LRN eddy-viscosity models. An overestimation of turbulence length scales gives an under-prediction of ε, which, in turn, over-predicts the turbulence energy. As a result, the near-wall heat transfer rate is enhanced. With the Yap term, however, the trend is opposite: the $\overline{\text{Nu}}$ is under-predicted by about 33 percent, which is consistent with the local Nu distributions shown in Figures 5 and 9.

The inclusion of non-linear stress-strain relation slightly improves the heat transfer rate, but still the $\overline{\mathrm{Nu}}$ is under-predicted by 24 percent. When the conjugate heat transfer approach is adopted, the predicted $\overline{\mathrm{Nu}}$ is in a better agreement with the experimental value compared to the prescribed heat flux approach (1.46 for the conjugate heat transfer approach and 1.36 for the prescribed heat transfer approach). However, even with the former approach, the $\overline{\mathrm{Nu}}$ is still 28 percent lower than the experimental data.

The $\overline{\mathrm{Nu}}$ predicted by the HRN k-ε model with the Yap term is only 7 percent lower than the experimental data. However, Figure 9 shows that the HRN model under-predicts the Nu distribution along the rib faces and over-predicts the Nu distribution along the channel bottom wall. This suggests that even if the $\overline{\mathrm{Nu}}$ may be well predicted, it does not necessarily mean that the local Nu distribution is entirely correct.

Since the HRN k-ε model with the Yap term predicts the closest $\overline{\mathrm{Nu}}$ to the experimental result, simulations were performed using this model for a range of Reynolds numbers ranging from 12,600 to 37,200 to obtain the correlation

$$\overline{\mathrm{Nu}}/\mathrm{Nu}_s = 0.0015\,\mathrm{Re}^{0.7553} \tag{49}$$

Figure 10 shows that the heat transfer is enhanced as the Reynolds number increases. This is reasonable since more energy is transferred from the mean flow to turbulence, which augments the heat transfer rate.

5. Conclusions

In the present study, both the high-Reynolds number and low-Reynolds number forms of the k-ε turbulence model, combined with a length-scale correction term in the ε-equation – the Yap term – were adopted to predict the heat transfer rate for a fully-developed flow in a ribbed channel heated at the bottom wall, in which massive flow separation occurs. In addition to the conventional linear stress-strain relation, a non-linear stress-strain relation truncated at the quadratic level with an eddy viscosity sensitized to the strain-rate and vorticity invariants (S and Ω) was also employed to investigate the effect of turbulence anisotropy on the predictions of mean-flow, turbulence quantities and local heat transfer rate. Thermal boundary conditions at fluid-solid interfaces were handled by the use of the prescribed heat flux approach and the conjugate heat transfer approach. The results of this investigation allow the following conclusions to be drawn

(1) For a massively separated flow, the inclusion of the Yap term in both the HRN and LRN models returns reasonably good predictions of the mean-velocity within the separation regions. Without the Yap term, however, the sizes of recirculation zones ahead and behind the rib are significantly under-predicted (not shown).

(2) The boundary-layer thickness on the rooftop of the rib is under-predicted by all turbulence models examined here, which is consistent with other earlier investigations using different turbulence models. This might be an indication of three-dimensionality in the experiment, which cannot be captured by the present two-dimensional calculations.

(3) The employment of non-linear stress-strain relation allows turbulence anisotropy to be predicted (only u'_{rms} is shown here). However, the level of

u'_{rms} is too low, which might be due to the adoption of C_μ in equation (7), which is a function of S and Ω instead of a constant 0.09, suppressing the turbulence-energy generation term P_k and, hence, u'_{rms}.

(4) The treatment of thermal boundary conditions using the conjugate heat transfer approach allows the correct heat flux at solid-fluid interfaces to be modeled. It is found that, if the thermal conductivity ratio of solid to fluid λ' is of the order of 100 or higher, its effect on the predicted Nu distribution is insignificant. Although this approach is computationally intensive, it does give better prediction in terms of $\overline{Nu}$ than the simple prescribed heat flux approach.

References

Bredberg, J. and Davidson, L. (1999), "Prediction of flow and heat transfer in a stationary two-dimensional rib roughened passage using low-Re turbulent models", paper presented at the Third European Conference on Turbomachinery, IMech C557/074/99, London.

Drain, L.E. and Martin, S. (1985), "Two-component velocity measurements of turbulent flow in a ribbed-wall flow channel", paper presented at the International Conference on Laser Anemometry – Advances and Applications, Manchester, pp. 99-112.

Jayatilleke, C.L.V. (1969), "The influence of Prandtl number and surface roughness on the resistance of the laminar sublayer to momentum and heat transfer", *Progress in Heat and Mass Transfer*, Vol. 1, pp. 193-329.

Jones, W.P. and Launder, B.E. (1972), "The prediction of laminarization with a two-equation model of turbulence", *International Journal of Heat and Mass Transfer*, Vol. 15, pp. 301-14.

Launder, B.E. and Spalding, D.B. (1974), "The numerical computation of turbulent flows", *Computer Methods in Applied Mechanics and Engineering*, Vol. 3, pp. 269-89.

Leonard, B.P. (1979), "A stable and accurate convective modeling procedure based on quadratic upstream interpolation", *Computer Methods in Applied Mechanics and Engineering*, Vol. 19, pp. 59-98.

Lien, F.S. and Leschziner, M.A. (1999), "Computational modeling of a transitional 3d turbine-cascade flow using a modified low-re k-ε model and a multi-block scheme", *International Journal of Computational Fluid Dynamics*, Vol. 12, pp. 1-15.

Lien, F.S., Chen, W.L. and Leschziner, M.A. (1996), "A multi-block implementation of a non-orthogonal collocated finite volume algorithm for complex turbulent flows", *International Journal for Numerical Methods in Fluids*, Vol. 23, pp. 567-88.

Liou, T.M., Hwang, J.J. and Chen, S.H. (1993), "Simulation and measurement of enhanced turbulent heat transfer in a channel with periodic ribs on one principal wall", *International Journal of Heat and Mass Transfer*, Vol. 36 No. 2, pp. 507-17.

Manceau, R., Parneix, S. and Laurence, D. (2000), "Turbulent heat transfer predictions using the $\bar{v}^2$-f model on unstructured meshes", *International Journal of Heat and Fluid Flow*, Vol. 21, pp. 320-8.

Patankar, S.V. (1978), "A numerical method for conduction in composite materials, flow in irregular geometries, and conjugate heat transfer", *Proceedings of the Sixth International Heat Transfer Conference*, Vol. 3, pp. 297-302.

Patankar, S.V. and Spalding, D.B. (1972), "A calculation procedure for heat, mass and momentum transfer in three-dimensional parabolic flows", *International Journal of Heat and Mass Transfer*, Vol. 15, pp. 1787-806.

Patankar, S.V., Liu, C.H. and Sparrow, E.M. (1977), "Fully developed flow and heat transfer in ducts having streamwise-periodic variations of cross-sectional area", *Journal of Heat Transfer*, Vol. 99, pp. 180-6.

Pope, S.B. (1975), "A more general effective-viscosity hypothesis", *Journal of Fluid Mechanics*, Vol. 72, pp. 331-40.

Rhie, C.M. and Chow, W.L. (1983), "Numerical study of the turbulent flow past an airfoil with trailing edge separation", *AIAA Journal*, Vol. 21 No. 11, pp. 1525-32.

Shih, T.H., Zhu, J. and Lumley, J.L. (1993), "A realizable Reynolds stress Algebraic equation model", *NASA Technical Memorandum*, 105993.

Speziale, C.G. (1987), "On non-linear k-l and k-ε models of turbulence", *Journal of Fluid Mechanics*, Vol. 178, pp. 459-75.

Tsai, W.B., Lin, W.W. and Chieng, C.C. (2000), "Computation of enhanced turbulent heat transfer in a channel with periodic ribs", *International Journal of Numerical Methods for Heat and Fluid Flow*, Vol. 10 No. 1, pp. 47-66.

Wang, Y. and Vafai, K. (1999), "Heat transfer and pressure loss characterization in a channel with discrete flush-mounted and protruding heat sources", *Experimental Heat Transfer*, Vol. 12, pp. 1-16.

Yap, C. (1987), "Turbulent heat and momentum transfer in recirculating and impinging flows", PhD thesis, Faculty of Technology, University of Manchester, Manchester.

Young, T.J. and Vafai, K. (1998a), "Convective cooling of a heated obstacle in a channel", *International Journal of Heat and Mass Transfer*, Vol. 41, pp. 3131-48.

Young, T.J. and Vafai, K. (1998b), "Convective flow and heat transfer in a channel containing multiple heated obstacles", *International Journal of Heat and Mass Transfer*, Vol. 41, pp. 3279-98.

Young, T.J. and Vafai, K. (1999), "Experimental and numerical investigation of forced convective characteristics of arrays of channel mounted obstacles", *ASME Journal of Heat Transfer*, Vol. 121, pp. 34-42.